

ORIGINAL ARTICLE

Anita Patel · Gautam Pulugundla  · Sergey Smolentsev ·
Mohamed Abdou · Rajendraprasad Bhattacharyay

Validation of numerical solvers for liquid metal flow in a complex geometry in the presence of a strong magnetic field

Received: 23 January 2017 / Accepted: 17 October 2017 / Published online: 14 November 2017
© Springer-Verlag GmbH Germany 2017

Abstract Following the magnetohydrodynamic (MHD) code validation and verification proposal by Smolentsev et al. (Fusion Eng Des 100:65–72, 2015), we perform code to code and code to experiment comparisons between two computational solvers, FLUIDYN and HIMAG, which are presently considered as two of the prospective CFD tools for fusion blanket applications. In such applications, an electrically conducting breeder/coolant circulates in the blanket ducts in the presence of a strong plasma-confining magnetic field at high Hartmann numbers, Ha (Ha^2 is the ratio between electromagnetic and viscous forces) and high interaction parameters, N (N is the ratio of electromagnetic to inertial forces). The main objective of this paper is to provide the scientific and engineering community with common references to assist fusion researchers in the selection of adequate computational means to be used for blanket design and analysis. As an initial validation case, the two codes are applied to the classic problem of a laminar fully developed MHD flows in a rectangular duct. Both codes demonstrate a very good agreement with the analytical solution for Ha up to 15,000. To address the capabilities of the two codes to properly resolve complex geometry flows, we consider a case of three-dimensional developing MHD flow in a geometry comprising of a series of interconnected electrically conducting rectangular ducts. The computed electric potential distributions for two flows (Case A) $Ha = 515$, $N = 3.2$ and (Case B) $Ha = 2059$, $N = 63.8$ are in very good agreement with the experimental data, while the comparisons for the MHD pressure drop are still unsatisfactory. To better interpret the observed differences, the obtained numerical data are analyzed against earlier theoretical and experimental studies for flows that involve changes in the relative orientation between the flow and the magnetic field.

Keywords Numerical validation · Magnetohydrodynamics · Fusion blankets · Strong magnetic fields

1 Introduction

Blankets, in particular a liquid metal (LM) blanket, is a principal component of a fusion nuclear power system with broadly three fundamental functions: (1) breeding tritium fuel required for a self-sufficient deuterium-tritium nuclear reaction, (2) absorption of neutrons from the plasma to convert their energy into heat and (3) cooling the blanket structure and the breeder zone [2]. To meet the associated requirements, a number of LM blanket concepts have been proposed. Among them, those utilizing eutectic alloy lead lithium (PbLi) as

Communicated by Oleg Zikanov.

G. Pulugundla (✉) · S. Smolentsev · M. Abdou
Center for Fusion Science and Technology, University of California Los Angeles (UCLA), Los Angeles, CA 90095, USA
E-mail: gautam@fusion.ucla.edu

A. Patel · R. Bhattacharyay
Institute of Plasma Research (IPR), Gandhinagar, Gujarat 382428, India
E-mail: anipatel2009@gmail.com

breeder/coolant attract the most attention due to their potentially high thermal efficiency and higher safety standards compared to other LM blanket concepts [3]. The most promising PbLi blanket concepts proposed in the recent past are dual-coolant lead-lithium (DCLL), helium-cooled lead lithium (HCLL), self-cooled lead-lithium (SCLL) and water-cooled lead-lithium (WCLL) blanket [2]. Recently, another blanket concept called lead-lithium-cooled ceramic breeder (LLCB) was proposed in India [4] that utilizes PbLi as a coolant of the ceramic pebble breeding zone and as a tritium breeder. In spite of the variations in the LM blanket concepts and designs, the common feature in all of them pertains to the fact that the LM flowing in the blanket ducts experiences strong magnetohydrodynamic (MHD) effects [5] due to its interaction with the strong plasma-confining magnetic field. The qualitative and quantitative analysis of any of these MHD effects is rendered profoundly difficult due to a combination of very high parameter values and complex flow configurations such as ducts, expansions, contractions, elbows and manifolds. Therefore, any effort to design a new LM blanket or to improve existing blanket designs would involve a thorough investigation of the three-dimensional effects associated with MHD flows in complex geometries. As an example, the total pressure drop, which is a very important consideration of any LM blanket, as well as the related flow structure, has to be calculated with sufficient accuracy for different geometrical configurations.

Presently in blanket flows, the 3D MHD pressure drop Δp_{3D} associated with the complex flow geometry is computed with the help of the commonly used empirical correlation suited for both hydrodynamic and MHD flows [6]:

$$\Delta p_{3D} = \xi \left(\frac{1}{2} \rho U_0^2 \right), \quad (1)$$

where U_0 is the characteristic velocity scale, ρ is the density of the fluid and ξ is the local pressure drop coefficient. In case of MHD flows in a strong magnetic field, the experimental data suggests that the pressure drop coefficient is directly proportional to the interaction parameter N , i.e., $\xi = kN$. The proportionality coefficient k is strongly dependent on the flow geometry and can be evaluated from the experimental data. Under conditions of a uniform magnetic field, this coefficient varies in the range from 0.2 to 2 as suggested in [3,7] for different flow geometries. The choice of k in many practical situations is to a major degree subjective, and it can be also lower than 0.2. Typically, higher values of k can be recommended for flows of higher geometrical complexity, such as a manifold, where the liquid is distributed from a feeding pipe into several individual ducts experiencing strong flow-opposing electromagnetic forces.

In the past, analytical, numerical and experimental work produced quite a good understanding of MHD flows in simple to relatively complex flow geometries [8–12]. However, each of those investigations were either restricted to low values of flow parameters or required special modeling by different approximate methods and rather expensive experiments. Fortunately, recently the development of new effective parallel MHD codes, including research and commercial computational fluid dynamics (CFD) codes, has substantially increased the use and effectiveness of computations as the predictive capability tool for blanket design and analysis due to the ability of these new codes to handle complex geometry flows in a strong magnetic field. In spite of these advances in computational engineering, all CFD solvers still need to be verified and validated for the specific conditions of MHD flows in a fusion blanket.

In fact the need and importance of such an activity was elucidated in a recent work by Smolentsev et al. [1], where an international campaign was launched with an aim to encourage researchers to perform benchmarking work on the widely used commercial and research CFD codes for several predetermined MHD flow cases that are important for fusion research. However, in those suggested benchmark cases there was no consideration given to MHD flows in complex geometries. Therefore in this work, as a part of the scientific collaboration between the University of California (UCLA) and the Indian Institute of Plasma Research (IPR) on fusion blanket development, we endeavor to validate two CFD solvers, HIMAG and FLUIDYN (which are the main blanket design and analysis tools used at UCLA and IPR correspondingly), for a LM flow in a complex geometry of interconnected rectangular ducts exposed to a spatially uniform magnetic field. For such a configuration, the numerical results are compared with experiments [13,14]. We also use existing theoretical studies as a means of understanding the flow in different subsections of the entire flow geometry. Although HIMAG has been validated for several complex geometry flows in the past, FLUIDYN has not been. Moreover, the proposed benchmark case of a flow in an interconnected rectangular ducts has additional features compared to the existing flow configurations such as MHD flow in a fringing magnetic field or MHD flow in a sudden expansion. From this point of view, the computations performed in this study can be considered as a validation of both codes.

The paper is organized as follows. Sect. 2 introduces the mathematical model. The two codes and associated numerical methods are described in Sect.3. Results of the first test case for fully developed MHD flows are

presented in Sect. 4. In Sect. 5, numerical results from the solvers are presented for the case of a three-dimensional developing MHD flow in a system of interconnected ducts, which is the key validation case in this study. In the same section, the numerical results are compared with theoretical predictions and experiments. This is finally followed by conclusions and suggestions for future work in Sect. 6.

2 Governing equations

For incompressible and viscous LM flows in fusion blankets, following the low magnetic Reynolds number assumption ($Re_m = U_0 L / \eta \ll 1$), the MHD governing equations can be written as follows [15],

Conservation of momentum

$$\frac{\partial \mathbf{U}}{\partial t} + (\mathbf{U} \cdot \nabla) \mathbf{U} = -\nabla p + \frac{1}{Re} \nabla^2 \mathbf{U} + \frac{Ha^2}{Re} (\mathbf{j} \times \mathbf{B}), \quad (2)$$

Ohm's law

$$\mathbf{j} = -\nabla \phi + \mathbf{U} \times \mathbf{B}, \quad (3)$$

and conservation of mass and electric charge

$$\nabla \cdot \mathbf{U} = 0, \quad \nabla \cdot \mathbf{j} = 0. \quad (4)$$

Combining Eqs. (3) and (4), we get the governing Poisson equation for the electrical potential ϕ :

$$\nabla^2 \phi = \nabla \cdot (\bar{\sigma} \mathbf{U} \times \mathbf{B}). \quad (5)$$

Here $\mathbf{U}(U, V, W)$ is the fluid velocity vector, $\mathbf{j}(j_x, j_y, j_z)$ is the vector of the electric current density, p is the pressure, t is the time and B_0 is the applied magnetic field. All the equations are written in dimensionless form, using the duct half-width L as the characteristic length scale. The associated scales of electric potential, current density and time are $U_0 B_0 L$, $\sigma U_0 B_0$ and L / U_0 , respectively. The equations include dimensionless parameters that express ratios between different physical processes or forces in the fluid. The hydrodynamic Reynolds number $Re = U_0 L / \nu$ is the ratio of inertial to viscous forces, $Ha = B_0 L \sqrt{\sigma / \rho \nu}$ is the Hartmann number, whose square is the ratio of electromagnetic to viscous forces. The ratio of electromagnetic to inertial forces is characterized by the interaction parameter $N = Ha^2 / Re$. The physical properties of the fluid are the density ρ , kinematic viscosity ν and electrical conductivity σ . The electric current entering the flow confining wall is controlled by the wall conductance ratio $C_w = \frac{\sigma_w t_w}{\sigma L}$, where σ_w is the electrical conductivity of the wall material and t_w is the wall thickness. Finally, $\bar{\sigma}$ indicates the dimensionless electrical conductivity given by σ / σ_w .

The boundary condition at the fluid wall interface is zero fluid velocity. Other boundary conditions include zero normal component of the induced current at the interface between the conducting wall and the non-conducting exterior domain leading to $\partial \phi / \partial n = 0$, and the inlet/outlet boundary conditions on the velocity field and electric potential that can vary depending on the flow configuration being simulated. In particular, a constant velocity inflow condition is specified at the inlet and the outlet is specified with zero pressure boundary condition. Wall boundary condition with no slip option is specified at all other boundaries.

The main objective of the numerical simulations is to determine the velocity, pressure, electric potential and the electric current density from Eqs. (2–5) using the above boundary conditions.

3 Numerical method

The two numerical solvers employed in this work are HIMAG and FLUIDYN. Both are capable of solving the MHD flow problems on both structured and unstructured computational grids. The characteristic features of each code are presented below.

3.1 HIMAG

HyPerComp incompressible MHD solver for arbitrary geometry (HIMAG) is a three-dimensional unstructured grid-based MHD flow solver developed by a US software company named HyPerComp, with support from UCLA [16]. The numerical approach is based on finite-volume discretization using a collocated arrangement (all unknowns are located at the cell centers) with second-order accuracy in space and time. The MHD part of the solver incorporates the electric potential formulation with a possibility to simulate multi-material domains, e.g., the induced electric currents closing-in through conducting solid walls. The mass conservation is satisfied, and the pressure field is evaluated using a four-step projection method with semi-implicit Crank–Nicolson formulation for the convective and diffusion terms. A charge conserving consistent scheme [17] is applied to Eqs. (4) and (3) to accurately compute the electric potential and the electric current density at high Hartmann numbers. Given the unstructured nature of the solver, multiple strategies are employed to account for mesh skewness and non-orthogonality. Finally, the solver algorithms are parallelized using MPI architecture, thereby making the solver capable of being run on large computational clusters.

3.2 FLUIDYN

FLUIDYN is an MPI parallelized general purpose multi-physics software that is designed to perform CFD simulations on a wide range of physical processes and engineering problems. In an earlier study, 3D thermo-fluid MHD analysis was performed using FLUIDYN for a simple problem of flow in a straight duct [18] and in this work we extend it to more complex flow geometries. Similar to HIMAG, the numerical approach in FLUIDYN is based on finite-volume discretization using a collocated scheme. The solver employs the Semi-Implicit Method for Pressure Linked Equation (SIMPLE) algorithm proposed in [19] for pressure velocity coupling. This algorithm is based on a predictor–corrector approach, which employs the relationship between velocity and pressure corrections to enforce mass conservation and to obtain the pressure field [20]. Identical to HIMAG, a charge conservation scheme is used in FLUIDYN to accurately compute the Lorentz force density term. Subsequently, all the spatial derivatives for the convective terms are solved using a second-order upwind scheme and for the diffusive terms using a second-order central difference scheme.

4 Case 1: Fully developed MHD flow in a straight square duct

The first benchmark problem addresses a steady fully developed laminar LM flow in a rectangular duct of cross section $2b \times 2b$ and length L subject to a uniform transverse magnetic field as shown in Fig. 1. This classical 2D MHD problem dates back to studies by Shercliff [21] for a non-conducting duct and by Hunt [22] for a duct with electrically conducting walls. It is well known that such flow configuration involves formation of two Hartmann boundary layers at the walls perpendicular to the magnetic field with the thickness scaling as $1/Ha$, two side (Shercliff) layers at the walls parallel to the magnetic field scaling as $1/Ha^{1/2}$ and the core region where the velocity is almost uniform. If the duct walls are electrically conducting, the flow forms high-velocity jets near the sidewalls also scaling in width as $1/Ha^{1/2}$ (“M-shaped” velocity profile).

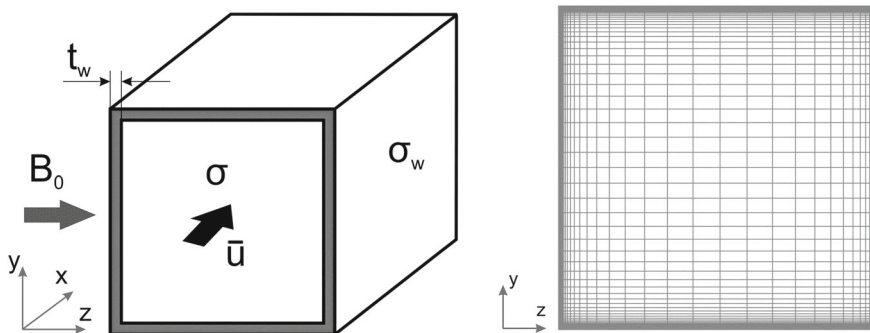


Fig. 1 Schematic of the fully developed flow in a straight square duct (left) together with the non-uniform grid in the duct cross section (right) employed in the numerical computations

Table 1 Dimensionless flow rate Q computed through 2D numerical simulations of fully developed laminar MHD flow with both insulating and conducting ($C_w = 0.01$) walls using HIMAG and FLUIDYN

Flow	Hartmann number	Q FLUIDYN (2D approach)	Q HIMAG (2D approach)	Q analytical
Insulating duct (A1)	500	7.678×10^{-3}	7.724×10^{-3}	7.680×10^{-3}
	5000	7.903×10^{-4}	7.934×10^{-4}	7.902×10^{-4}
	15,000	2.648×10^{-4}	2.663×10^{-4}	2.648×10^{-4}
Conducting duct (A2)	500	1.405×10^{-4}	1.407×10^{-4}	1.405×10^{-4}
	5000	1.909×10^{-5}	1.909×10^{-5}	1.907×10^{-5}
	15,000	2.432×10^{-6}	2.430×10^{-6}	2.425×10^{-6}

Hartmann numbers for the simulations are 500, 5000 and 15,000, and the results of these are compared with analytical solutions from [21] and [22]

In this work, we investigate two sub-cases, where (A1) all four walls are non-conducting and (A2) two walls perpendicular to the magnetic field are conducting and two other walls are non-conducting. For both these cases, the main objective of the numerical simulations is to evaluate the dimensionless flow rate expressed as,

$$Q = \iint_A U \, dy \, dz, \quad (6)$$

$$U = \frac{\mu u}{b^2 \left(\frac{-dp}{dx} \right)}, \quad (7)$$

where $\left(\frac{dp}{dx} \right)$ is the pressure gradient in the fluid.

For the computations in both HIMAG and FLUIDYN, two different numerical approaches can be employed, namely a full 3D approach and a simplified 2D approach. In a full 3D approach, simulations are performed by using the boundary conditions presented in Sect. 2 for MHD flow in a long duct where the flow is allowed to naturally develop and reach a fully developed state. As can be expected, for a such a configuration the duct needs to be sufficiently long for the flow to reach a fully developed state without the influence of either the inlet or the outlet. However, for simulating fully developed flows both the codes provide an opportunity to use a simplified 2D approach. It basically involves making $\left(\frac{dp}{dx} \right)$ constant. This avoids the need to solve the pressure Poisson equation. For the momentum equations, the convective terms together with the pressure gradient in y and z directions are put to zero. All these simplified governing equations are solved using the Neumann boundary condition for all variables both at inlet and outlet of the duct. We tested both the approaches for Hartmann number 500 and obtained identical grid-independent results. In particular, due to the simplicity of the 2D numerical modeling strategy, the computational time needed to reach a converged flow solution, $|Q^{n+1} - Q^n| / |Q^n| < 10^{-10}$, is much lower (< 2 h) than the 3D approach. Therefore, we employed the 2D approach to perform parametric studies for the remaining two Hartmann numbers 5000 and 15,000.

The numerical results from both the codes are then compared to the analytical solutions. From these results, shown in Table 1, it can be observed that the non-dimensional flow rates obtained from HIMAG and FLUIDYN agree very well with those from the analytical solution for all Hartmann numbers for both conducting and non-conducting duct walls with an error of less than 1%.

5 Case 2: Three-dimensional MHD flow in a complex geometry

The benchmarking problem presented in Sect. 4 on a fully developed MHD flow in a square duct is a simple and necessary case for the code validation but not a sufficient one. In fact, in order to adequately test a numerical MHD code for generic flow configurations, we need to consider a more general case when the flow geometry is complex such that the 3D features become essential. Such an endeavor is particularly important because of its relevance to the design of LM fusion blankets, where complex flow geometries are employed. That is why, in this section, we focus on the numerical modeling of a three-dimensional LM flow in a complex geometry of five interconnected electrically conducting rectangular ducts subject to a spatially uniform magnetic field as shown in Fig. 2. The numerical results are then compared between the two codes and also against the experiments performed jointly by IPR and IPUL (Institute of Physics of University of Latvia) in Riga, Latvia [13, 14].

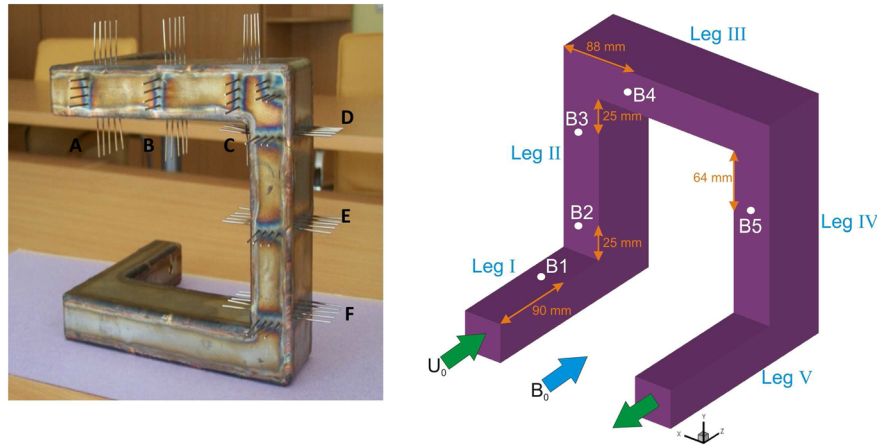


Fig. 2 (Left) photograph of the experimental duct illustrating the locations of the pins (from A to F) used to measure the wall electric potential. (Right) schematic of the geometry used for the numerical simulations illustrating the corresponding experimental locations of the pressure taps B1, B2, B3, B4 and B5. The flow parameters used in this work are summarized in Table 2

Table 2 Parametric space in the experiments in terms of non-dimensional control parameters. These values are used as input for the numerical simulations

Case	C_w	Re	Ha	N	Ha/Re	\sqrt{Ha}/Re
A	0.1574	82,719	515	3.2	6.2×10^{-3}	2.7×10^{-4}
B	0.1574	66,404	2059	63.8	3.1×10^{-2}	6.8×10^{-4}

5.1 Physical experiment

In the experiments, eutectic alloy PbLi was used as the working LM, which was pumped through the complex geometry test section shown on the left of Fig. 2, using a variable-speed electromagnetic pump. The external uniform magnetic field was produced with a superconducting helium-cooled solenoid of inner diameter 300 mm and axial length of 1000 mm, which provides a maximum magnetic field strength of 4T. The corresponding non-dimensional parameters Ha , Re and N are summarized in Table 2. The LM is supplied to the test section through the inlet pipe, which firstly flows horizontally through inlet leg I of the test section, which is parallel to the magnetic field and then makes a 90° turn and flows vertically through leg II perpendicular to the magnetic field. The change in the flow direction between legs I and II of the test section occurs in the plane parallel to the magnetic field. At the exit of leg II, the flow makes another 90° turn in the plane perpendicular to the magnetic field and flows horizontally through leg III, which is also perpendicular to the applied magnetic field. Other two legs, IV and V, are symmetric to legs II and I, but the flow direction is opposite. Similar to the inlet pipe, the flow comes out from the test section through the outlet pipe connected to leg V. The exact dimensions of each of these legs in the experiment are illustrated in Fig. 3.

The experimental measurements covered a pressure distribution along the flow path as well as electric potential distribution on the outer surface of the test section. The pressure distribution was measured at locations B1, B2, B3 and B4, where the pressure taps were mounted on the duct wall, as shown on the right of Fig. 2. A special indirect pressure measurement technique was employed in the experiment, where the LM pressures are obtained by measuring the cover gas pressure of small expansion tanks connected to the test section. The electric potential distribution on the wall of the test section was measured at six locations A, B, C, D, E and F. At each cross-sectional location, there are four pins on the Hartmann walls and five pins on the sidewalls. Each of these stainless steel electric potential pins is of diameter 1.2 mm and is welded to the test section as shown on the left of Fig. 2. The PbLi flow rate in the test section was measured with the calibrated Faraday-type electromagnetic flowmeter placed outside the solenoid.

The pressure and electric potential measurements were used to compare with the numerical data computed by the two reference MHD codes HIMAG and FLUIDYN. For the computation of 3D MHD flow in this complex geometry in both FLUIDYN and HIMAG, an identical block structured grid is employed. The walls of the geometry have been meshed uniformly with 5 elements along the thickness. A total of 10 and 8 grid

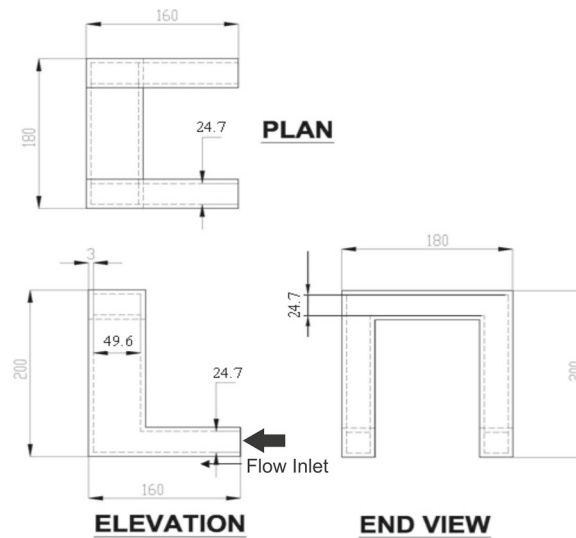


Fig. 3 Schematic of the dimensions of different sections of the experimental geometry. All the value illustrated are in mm

points are employed in the side layer and the Hartmann layer, respectively. A total of 1.6 million grid points are used in the analysis.

5.2 Anticipated flow phenomena

The associated MHD problem is quite complicated from the standpoint of both the numerical simulations and the physical interpretations of the results as the geometry involves changes in the relative orientation between the flow and the magnetic field. In particular, at the inlet and the outlet ducts of the test section (legs I and V in Fig. 2, right), the magnetic field is parallel to the main flow direction. This makes the flow in these two legs almost hydrodynamic in nature as there is no direct action of the Lorentz force on the main (axial) velocity component. Moreover, at such high Reynolds numbers, the flow in these two legs is invariably turbulent. In legs II, III and IV, the flow is perpendicular to the applied magnetic field, resulting in a very strong MHD interaction compared to legs I and V. It is useful to compare the parameters Ha/Re (represents Reynolds number based on the thickness of the Hartmann layer as the characteristic length) and \sqrt{Ha}/Re (represents Reynolds number based on the thickness of the Shercliff layer as the characteristic length) against the critical values obtained for the flows in a non-conducting duct subject to a transverse magnetic field. These critical values are $1/380 = 0.0026$ and $1/65 = 0.0153$ correspondingly [23]. Therefore, the flow in the Hartmann layers of legs II, III and IV is laminar, while the side layer flows are likely turbulent, possibly taking the form of quasi-two-dimensional ($Q2D$) turbulence [24]. Notice that these critical values were obtained for fully developed flows in a non-conducting duct such that more definite conclusions about the flow regimes in legs II, III and IV cannot be deduced from Ha/Re and \sqrt{Ha}/Re because of the unknown contributions of the electrically conducting walls and also of the flow development effects in the experiment. Furthermore, the presence of the corner regions between legs I and II, II and III, III and IV, and IV and V in the experimental test section may lead to recirculation or even locally stagnant flows. The physical complexity of the flow is also related to the high-velocity jets that can likely form at the sidewalls of the test section. Besides that, changes in the flow direction in the experimental test section occur both in the plane parallel to the magnet field (between legs I and II, and legs IV and V) and perpendicular to the field (between legs II and III, and III and IV). These two changes in the flow direction with respect to the applied magnetic field are known to have different effects on the flow structure and the MHD pressure drop.

Taking into account these anticipated flow phenomena and also location of the pressure taps and electric potential pins in the experiment, it is reasonable—when analyzing the computed data—to partition the entire complex flow geometry into three different sections and then consider them separately. As shown in Fig. 4, the first section is the L-bend that has pressure taps B1 and B2, where the flow turns at 90° in the plane parallel to the applied magnetic field (Fig. 4a). The second section that coincides with leg III of the test section represents

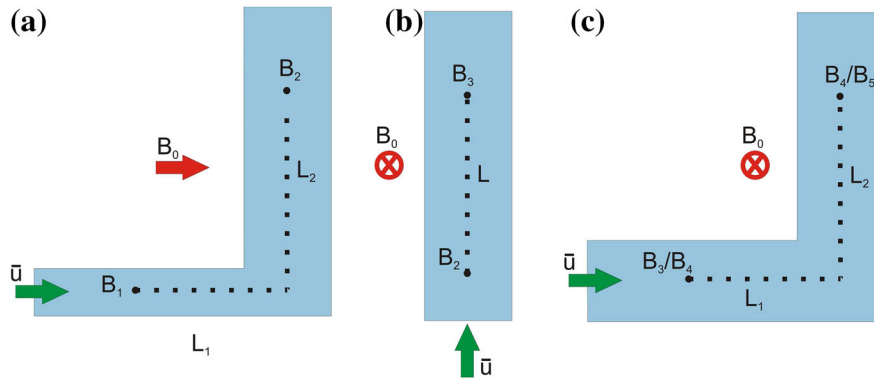


Fig. 4 Schematic illustrating the different subsections of the entire flow geometry: **a** section 1, **b** section 2 and **c** section 3. Such a partitioning is useful for understanding the basic MHD flow physics and for the computation of the pressure drop between different experimental pressure sensors

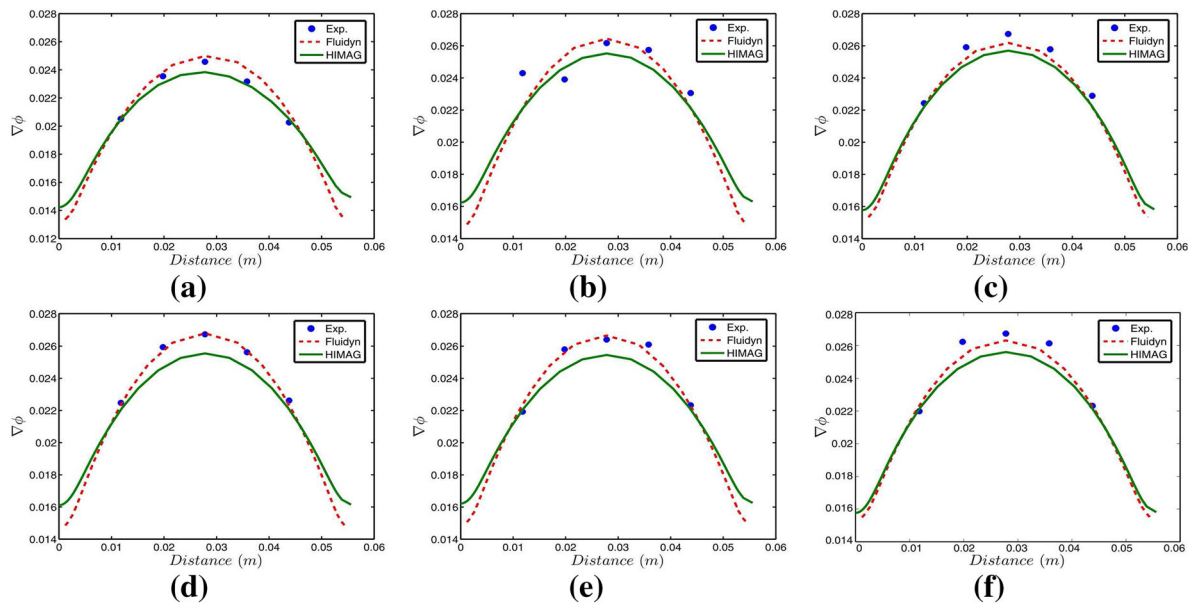


Fig. 5 Comparison of the electrical potential difference ($\Delta\phi$ in V) between the sidewalls of the geometry from HIMAG, FLUIDYN and experiments. Each of the graphs illustrate the values from all 5 potential pins at 6 different streamwise locations (from A to F) as shown in Fig. 2. The results demonstrate a good agreement between the numerical solvers and experiments

the MHD flow in a straight duct. The MHD pressure drop over this section is measured and computed between the two locations B2 and B3 (Fig. 4b). The last section is the U-bend (Fig. 4c) that includes two changes in the flow direction due to two right angle bends where the liquid flows perpendicular to the magnetic field. The pressure drop over this section is measured in the experiment between locations B3 and B4, and B4 and B5.

5.3 Comparison of the electric potential

We use the sidewall electrical potential as measured in the experiments at different streamwise locations to compare with computations as shown in Fig. 5. The potential difference ($\Delta\phi$) results from HIMAG and FLUIDYN agree reasonably well with each other and with the experiments. In particular, at location A, which is close to the junction between legs I and II, the measured values agree well with the numerical results for the case with higher Hartmann number. As can be expected, with the decrease in the Hartmann number, the deviation from the numerical values also increases. This could be due to the presence of higher corner turbulence in the flow in the bend at higher Reynolds number as the magnetic field is parallel to the flow. On the other hand, at locations B, C and E the measured ($\Delta\phi$) agrees well with the numerical results for all the

considered non-dimensional control parameters. This indicates that laminarization of the flow due to stronger MHD forces in the regions reasonably far away from the corners. Finally, at location D closer to the corner but not as close as location A, it can be seen from Fig. 5 that the numerical results differ a little from the experiments. However, this difference is not very strong given that the magnetic field is perpendicular to the flow in both the legs of the U-bend.

5.4 Comparison of the MHD pressure drop

Together with the electric potential, we compare the pressure drops for cases A and B at different locations in the LM flow obtained by measurements, numerical simulations of both HIMAG and FLUIDYN. It can be observed in Table 3 that the agreement among the experimental and numerical simulations produces mixed results. For Case A at a lower $Ha = 515$, the experimental results show a big discrepancy with the numerical results. However, the numerical results agree well with each other within a good degree of accuracy. This can be attributed mainly to two reasons: first of which stems from the small absolute value of Δp (around 1–8 kPa) at $Ha = 515$. As explained in [25], such small absolute values of Δp lead to a larger instrumentation error in indirect pressure measurement technique used in the experiment. The second source of discrepancy comes from the limitations of the numerical simulation techniques employed in both HIMAG and FLUIDYN as they have been developed specifically for laminar flows (in case of HIMAG, it was designed for MHD flows that are in a laminar state due to the strong MHD effect on suppression of turbulence). In the experiments, however, the Reynolds number is relatively high at $Ha = 515$ leading to a fully turbulent flow in the inlet and outlet regions of the duct and therefore to a higher error in the Δp comparison. As expected, for Case B at a higher $Ha = 2059$, the comparison is pretty good between experimental and both sets of numerical results. The details of the exact flow dynamics in different legs of the geometry are presented in Sects. 5.5–5.6.

To better understand the flow physics and to interpret the discrepancy between the numerical results and the experiments, we evaluate the pressure drop between different sensors using an existing fully developed theoretical estimate that was empirically obtained from experimental results in MHD flows in channels with electrically conducting walls [26],

$$\Delta p_{2D} = \left(\frac{C_w}{4/3 + C_w} \right) \sigma U_0 B_0^2 D, \quad (8)$$

where D is the flow length transverse to the magnetic field.

Usually in wall-bounded MHD flows, the total MHD pressure drop is understood to be a superposition of 2D and 3D effects. The 2D pressure drop is theoretically well understood as it is a result of cross-sectional electric currents dominant in fully developed MHD flows (Eq. 8). The 3D pressure drop (Eq. 1) is caused by the presence of axial electric currents in the flow that are relatively less understood as they are present in complex MHD flow configurations such as fringing magnetic fields, bends, expansions, etc. From the results shown in Table 3, it can be observed the 2D fully developed pressure drop alone is a lot higher than the total MHD pressure drop obtained through both experiments and 3D numerical simulations for all pressure sensor locations. This result is contrary to the traditionally held understanding of pressure superposition. A qualitative theoretical argument could perhaps be made for this disparity in pressure drop between the first two pressure sensors B1 and B2 as the flow here encounters a sudden expansion in cross section coupled with flow turning

Table 3 Comparison of the pressure difference (Δp) between the successive streamwise pressure sensors as evaluated from HIMAG, FLUIDYN, experiments and theoretical estimates for two different Cases A and B as listed in Table 2

Case	Approach	Pressure difference (B1–B2), Bar	Pressure difference (B2–B3), Bar	Pressure difference (B3–B4), Bar	Pressure difference (B4–B5), Bar
Case A	Experimental	0.0838	0.0322	0.0116	0.0717
	FLUIDYN	0.0155	0.0241	0.0276	0.0406
	HIMAG	0.0184	0.0172	0.0315	0.0403
	Theory (fully developed flow)	0.0378	0.0331	0.0491	0.0649
Case B	Experimental	0.1745	0.3803	0.2400	0.4394
	FLUIDYN	0.1781	0.2968	0.2638	0.4128
	HIMAG	0.1850	0.2456	0.3259	0.4362
	Theory (fully developed flow)	0.4854	0.4256	0.6308	0.8337

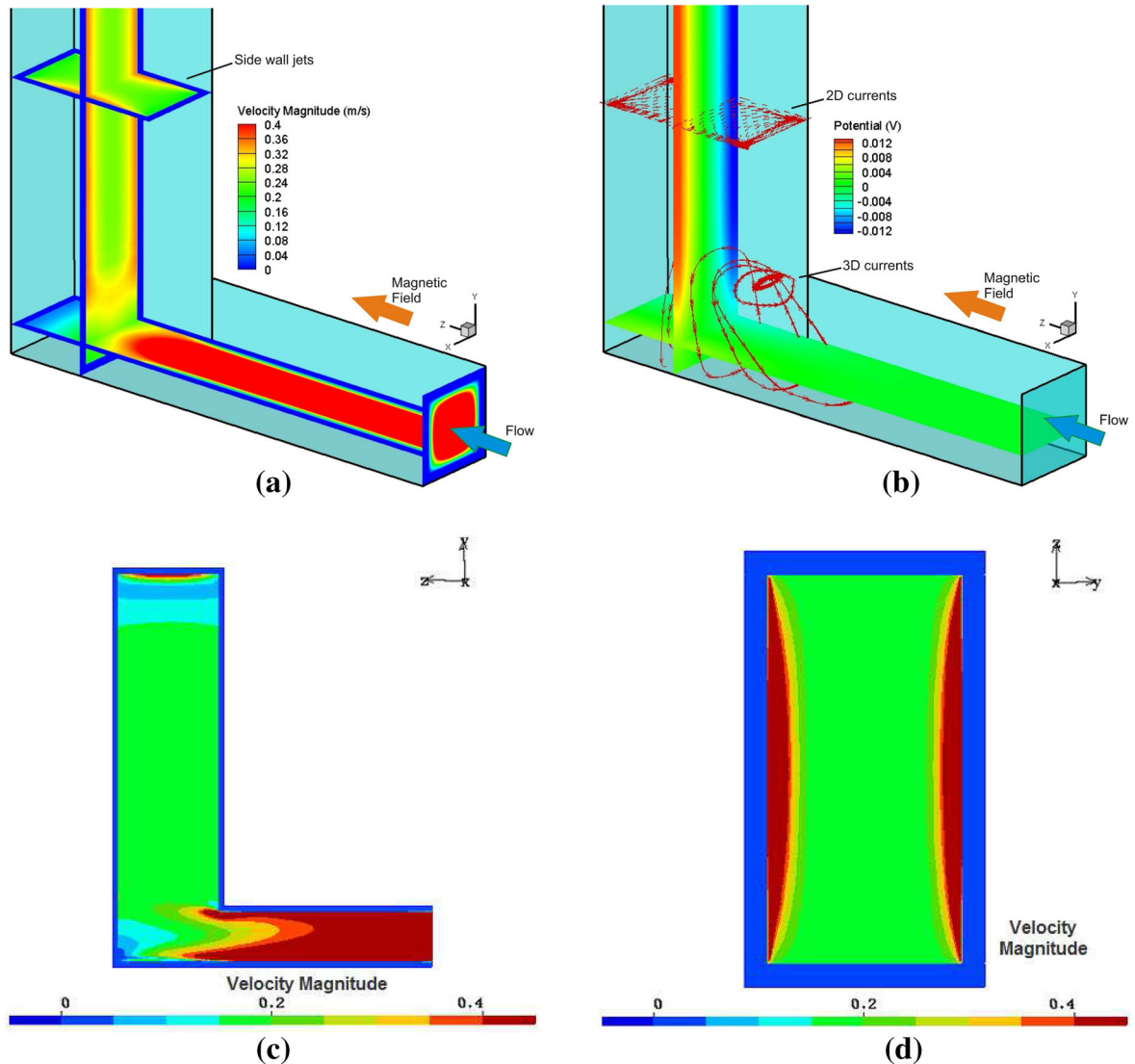


Fig. 6 **a** Contours of velocity magnitude on various planes inside the L-bend subsection of the flow geometry obtained from numerical simulations in HIMAG. **b** Contours of electric potential and current streamlines in the L-bend. Near the corners, the currents have a complicated 3D characteristic and further upstream they recover a 2D distribution in x - z planes. **c**, **d** Contours of velocity magnitude on middle y - z plane and on x - z plane far upstream from the L-bend corner obtained from numerical simulations in FLUIDYN. All the numerical results are from simulations performed at $Ha = 2059$, $Re = 66,404$ and $C_w = 0.1574$

from parallel to perpendicular direction with respect to the applied magnetic field. However, the pressure drop between all the other pressure sensor locations, where cross section in both the legs of the bend are same and the flow is always perpendicular to the magnetic field, should provide a better match with the fully developed pressure. In spite of this understanding, the 2D fully developed pressure drop seems to be higher between all pressure sensors irrespective of the flow sub-geometry and the magnetic field orientation. Therefore, the results from this study raise a fundamental question regarding the validity of the traditionally applied engineering estimate of the total MHD pressure drop in a complex geometry being a simple superposition of 2D and 3D pressure drops. In fact in the future, there is a strong need to theoretically prove the universality of this existing pressure superposition principle.

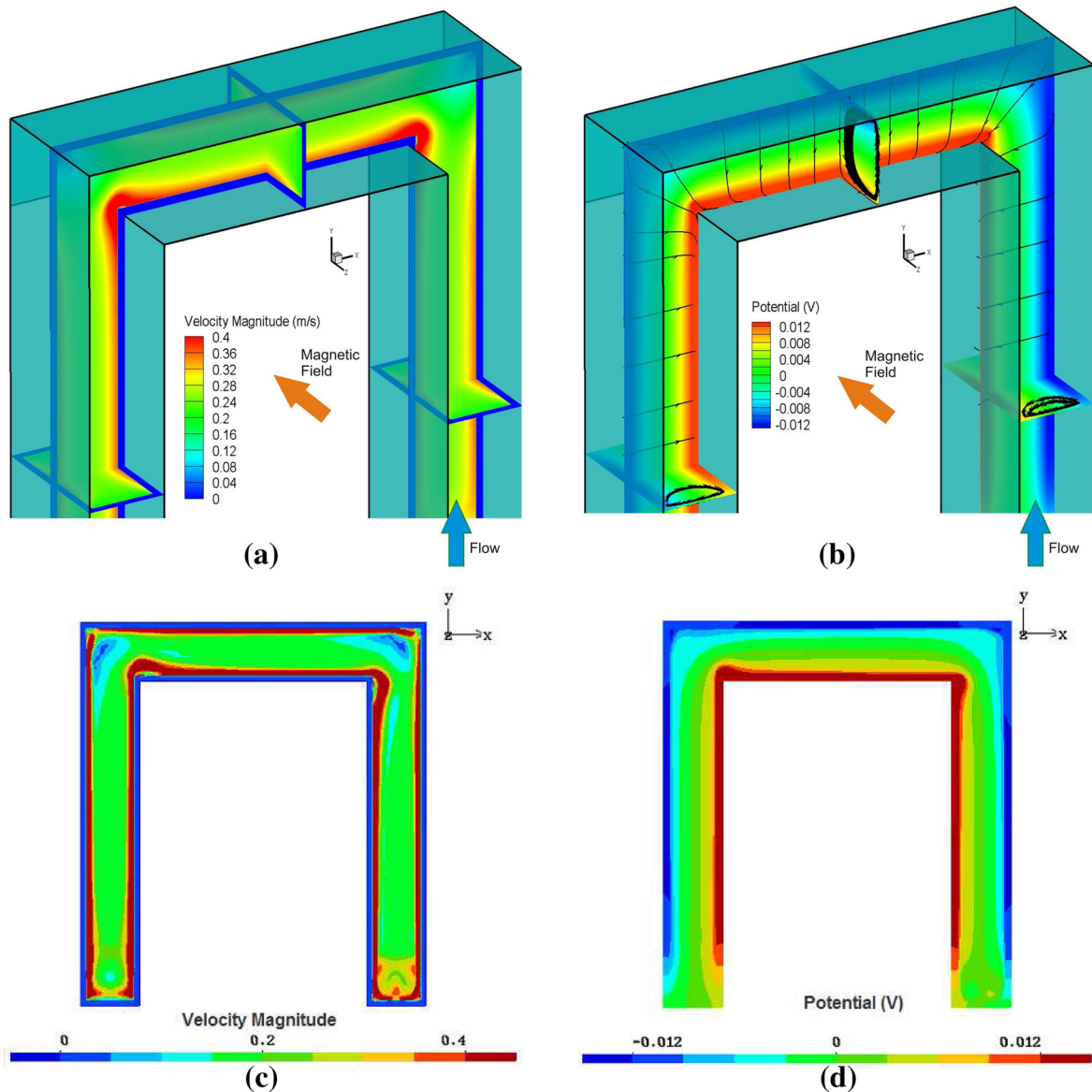


Fig. 7 Results as obtained from the numerical simulations performed at $Ha = 2059$, $Re = 66,404$ and $C_w = 0.1574$ in the U-bend region as the flow changes direction twice from leg II all the way to leg III through two 90° bends in the flow domain in the presence of a perpendicular magnetic field. **a, c** Illustrate the velocity magnitude distribution as computed in HIMAG and FLUIDYN (in the middle x - y plane), respectively, and **b, d** illustrate the electric potential distribution and electric current streamlines as computed in HIMAG and FLUIDYN (in the middle x - y plane), respectively

5.5 Flow in the first section: L-bend

In the sharp 90° L-bend (Fig. 4a), the flow turns from one duct with flow direction parallel to the magnetic field to the other duct with flow direction perpendicular to the magnetic field. MHD flow dynamics in L-bend configurations were investigated in many studies in the past [27,28], but the experimental and asymptotic inertia-less study by Steiglitz et al. [28] at high values of the interaction parameters was the most comprehensive in terms of its application to fusion relevant MHD flows. Therefore, we will try to extend their analysis to this section of our geometry.

The flow enters the first duct in a purely hydrodynamic state at a high Reynolds number of $Re = 66,404$ (see Fig. 6a, c). For such a configuration, the magnetic field has a limited effect on the fluid flow as it is parallel to the mean flow direction, and therefore, the field does not modify the base flow but only suppresses the

three-dimensional perturbations [29]. This suppression is dominant for Case B (see Table 2) the critical value for transition is $(Ha/Re)_{cr} = 0.025$ [30]. Although the numerical simulations in both FLUIDYN and HIMAG are performed without any turbulence model, an exact comparison in terms of degree turbulence suppression was not made as the experimental data for this leg is not available.

As the fluid approaches the second duct, here the flow is perpendicular to the magnetic field, an electrical potential difference is induced across the sidewalls in the fluid that drives electric currents in the cross section of the flow (Fig. 6b, d). This transition at the corner junction between the two ducts leads to the formation of an electric potential difference in the flow direction. A three-dimensional electric current is then ensued due to this potential difference as observed in the numerical simulation results of HIMAG and FLUIDYN. The streamwise component of the current results in a Lorentz force that drives fluid toward the sidewalls, thereby creating the well-known “M-shaped” velocity profile with sidewall jets and leads to a strong reduction in the core velocity in the second duct of the L-bend. As can be observed in Fig. 6, both HIMAG and FLUIDYN capture identically the flow features such sidewall jets, 3D electric currents very well. This complex flow dynamics has a profound impact on the total pressure drop between the pressure sensors $B1$ and $B2$ as seen in Sect. 5.4.

5.6 Flow in the second and third sections: U-bend

In this section, we analyze MHD flow in the combination of the legs II, III and IV which together make up a so-called U-bend geometry. Such configurations have been investigated in the past through works of Molokov and Bühler and Reimann et al. [31,32], where an inertia-less approximation ($N \gg Ha^{3/2}$) was used to numerically compute the MHD flow behavior with changing orientation between magnetic field and mean flow. However, in this work, throughout the U-bend the magnetic field is always perpendicular to the mean flow direction.

As the flow advances from the L-bend (see Sect. 5.5) in leg II, the “M-shaped” velocity profile becomes more developed and toward the end of that leg the velocity profile slowly becomes asymmetric with the maximum flow velocity near at the inner side wall jet. Therefore, near the transition between legs II and III, more flow rate is carried by the inner sidewall jet (see Fig. 7a, c). The main reason for this asymmetry is due to the axial currents that are caused by the creation of a streamwise potential gradient (see Fig. 7b, d). These axial current create an opposing Lorentz force that pushes the flow toward the inner wall. In addition to this MHD flow behavior, the geometric shape of the bend also leads to the formation of recirculation region upstream from the corner in leg III. All these flow features are accurately captured by both HIMAG and FLUIDYN (Fig. 7).

6 Conclusions

We performed numerical simulations using CFD codes HIMAG and FLUIDYN for MHD flows in complex flow geometries. The computations were intended to act as a numerical benchmark for future simulations at high Hartmann and Reynolds numbers in complex geometries similar to those employed for the design of nuclear fusion reactor blankets. The analysis was performed by comparing the numerical results from both codes with those obtained through experiments and well-known simple theoretical estimates for varying levels of complexity in terms of MHD flow behavior. For relatively simple flow configurations such as a steady fully developed MHD flow in a square duct, the numerical solvers produced identical results when compared with analytical solution. For MHD flow in a complex flow geometry with electrically conducting walls, the comparison studies demonstrated some interesting and promising results. In particular, there was a reasonably good agreement between all the numerical solvers and experiments for wall electrical potential measurements at different locations. On the other hand, the comparison of pressure drop demonstrated mixed results. At low interaction parameter, pressure drop computation by both numerical solvers agreed well with each other but the not with those from the experiments. However, at high interaction parameter all the three methods demonstrated reasonable agreement. This could be due to the limited accuracy of the experimental pressure measurement system at low absolute values of fluid pressure. The pressure drop results were also compared with fully developed theoretical estimates, and the comparison raised an important question regarding the validity of the assumption that the total MHD pressure drop in a complex geometry is a simple superposition of 2D and 3D pressure drops. Finally, the present work provides a good credibility baseline for future numerical simulations of MHD flows in complex geometry using HIMAG and FLUIDYN.

Acknowledgements Authors G.P, S.S, M.A thank the U.S. Department of Energy, Office of Science, Office of Fusion Energy Sciences, for financial support under the Award Number DE-FG02-86ER52123. All HIMAG simulations used the computational resources of Hoffman2 Shared Cluster provided by UCLA Institute for Digital Research and Education's Research Technology Group.

References

- Smolentsev, S., Badia, S., Bhattacharyay, R., Bühler, L., Chenj, L., Huang, Q., Jin, H.G., Krasnov, D., Lee, D.W., de les Valls, E.M., Mistrangelo, C., Munipalli, R., Ni, M.J., Pashkevich, D., Patel, A., Pulugundla, G., Satyamurthy, P., Snegirev, A., Sviridov, V., Swain, P., Zhouf, T., Zikanov, O.: An approach to verification and validation of MHD codes for fusion applications. *Fusion Eng. Des.* **100**, 65–72 (2015)
- Abdou, M., Morley, N.B., Smolentsev, S., Ying, A., Malang, S., Rowcliffe, A., Ulrickson, M.: Blanket/first wall challenges and required R&D on the pathway to DEMO. *Fusion Eng. Des.* **100**, 2–43 (2015)
- Smolentsev, S., Wong, C., Malang, S., Dagherand, M., Abdou, M.A.: MHD considerations for the dcll inboard blanket and access ducts. *Fusion Eng. Des.* **85**, 1007–1011 (2010)
- Kumar, E.R., Danani, C., Sandeep, I., Chakrapani, C., Pragash, N.R., Chaudhari, V., Rotti, C., Raole, P.M., Alphonsa, J., Deshpande, S.P.: Present understanding of MHD and heat transfer phenomena for liquid metal blankets. *Fusion Eng. Des.* **27**, 553–569 (1995)
- Smolentsev, S., Moreau, R., Buehler, L., Mistrangelo, C.: MHD thermofluid issues of liquid-metal blankets: phenomena and advances. *Fusion Eng. Des.* **85**, 1196–1205 (2010)
- Norajitra, P., Buehler, L., Buenaventura, A., Diegele, E., Fischer, U., Gordeev, S., Hutter, E., Kruesmann, R., Malang, S., Maisonnier, D., Orden, A., Reimann, G., Reimann, J., Vieider, G., Ward, D., Wasastjerna, F.: Conceptual design of the dual-coolant blanket within the framework of the EU power plant conceptual study (TW2-TPR-PPCS12). Final Report FZKA 6780. Forschungszentrum Karlsruhe GmbH (2003)
- Smolentsev, S., Moreau, R., Abdou, M.A.: Characterization of key magnetohydrodynamic phenomena in PbLi flows for the US DCLL blanket. *Fusion Eng. Des.* **83**, 771–783 (2008)
- Smolentsev, S., Morley, N.B., Abdou, M.A.: Code development for analysis of MHD pressure drop reduction in a liquid metal blanket using insulation technique based on a fully developed flow model. *Fusion Eng. Des.* **73**, 83–93 (2005)
- Bühler, L., Horanyi, S., Arbogast, E.: Experimental investigation of liquid-metal flows through a sudden expansion at fusion-relevant Hartmann numbers. *Fusion Eng. Des.* **82**, 2239–2245 (2007)
- Mistrangelo, C., Raffray, A.R., Team, A.: MHD analysis of dual coolant Pb-17Li blanket for ARIES-CS. *Fusion Sci. Technol.* **52**, 849–854 (2007)
- Messadek, K., Abdou, M.A.: Experimental study of MHD flows in a prototypic inlet manifold section of the DCLL test blanket module. *Magnetohydrodynamics* **45**(2), 233–238 (2009)
- Mistrangelo, C.: Topological analysis of separation phenomena in liquid metal flow in sudden expansions. Part 2. Magnetohydrodynamic flow. *J. Fluid Mech.* **674**, 132–162 (2011)
- Bhattacharyay, R., Patel, A., Ellappana, R., Swain, P.K., Satyamurthy, P., Kumar, S., Ivanov, S., Shishko, A., Platacis, E., Ziks, A.: Liquid metal MHD experimental activities for LLCB TBM development. *Fusion Eng. Des.* **88**, 2244–2250 (2013)
- Swain, P.K., Satyamurthy, P., Bhattacharyay, R., Patel, A., Shishko, A., Platacis, E., Ziks, A., Ivanov, S., Deshpande, A.V.: 3D MHD leadlithium liquid metal flow analysis and experiments in a test-section of multiple rectangular bends at moderate to high Hartmann numbers. *Fusion Eng. Des.* **88**, 2848–2859 (2013)
- Davidson, P.A.: *An Introduction to Magnetohydrodynamics*. Cambridge University Press, Cambridge (2001)
- Munipalli, R., Shankar, V., Ni, M.J., Morley, N.: Development of a 3-D incompressible free surface MHD computational environment for arbitrary geometries: HIMAG. DOE SBIR Phase-II Final Report (2003)
- Ni, M.J., Munipalli, R., Morley, N.B., Huang, P., Abdou, M.A.: A current density conservative scheme for incompressible MHD flows at low magnetic Reynolds number. Part II: on an arbitrary collocated mesh. *J. Comput. Phys.* **227**, 205–228 (2007)
- Patel, A., Bhattacharyay, R., Srinivasan, R., Rajendrakumar, E., Bhuyan, P., Satyamurthy, P., Swain, P., Goswami, K.: 3D thermo-fluid MHD simulation of single straight channel flow in LLCB TBM. *Fusion Eng. Des.* **87**, 498–502 (2012)
- Patankar, S.V., Spalding, D.B.: A calculation procedure for heat, mass and momentum transfer in three-dimensional parabolic flows. *Int. J. Heat Mass Trans.* **15**(10), 1787–1806 (1972)
- FLUIDYN-MP: Ver. 5.2.1: User's guide. FLUIDYN (2011)
- Shercliff, J.A.: Steady motion of conducting fluids in pipes under transverse magnetic fields. *Proc. Camb. Philos. Soc.* **49**, 136–144 (1953)
- Hunt, J.C.R.: Magnetohydrodynamic flow in rectangular ducts. *J. Fluid Mech.* **21**, 577–590 (1965)
- Smolentsev, S., Vetcha, N., Abdou, M.: Effect of a magnetic field on stability and transitions in liquid breeder flows in a blanket. *Fusion Eng. Des.* **88**, 607–610 (2013)
- Sommeria, J., Moreau, R.: Why, how, and when, MHD turbulence becomes two-dimensional. *J. Fluid. Mech.* **118**, 507–518 (1982)
- Li, F.C., Sutevski, D., Smolentsev, S., Abdou, M.: Experimental and numerical studies of pressure drop in pbli flows in a circular duct under non-uniform transverse magnetic field. *Fusion Eng. Des.* **88**, 3060–3071 (2013)
- Kirilov, I.R., Reed, C.B., Barleon, L., Miyazaki, K.: Present understanding of MHD and heat transfer phenomena for liquid metal blankets. *Fusion Eng. Des.* **27**, 553–569 (1995)
- Moon, T.J., Walker, J.S.: Liquid metal flow through a sharp elbow in the plane of a strong magnetic field. *J. Fluid. Mech.* **213**, 397–418 (1990)
- Stieglitz, R., Barleon, L., Bühler, L., Molokov, S.: Magnetohydrodynamic flow in a right-angle bend in a strong magnetic field. *J. Fluid Mech.* **326**, 91–123 (1996)

-
29. Zikanov, O., Krasnov, D., Boeck, T., Thess, A., Rossi, M.: Laminar-turbulent transition in magnetohydrodynamic duct, pipe, and channel flows. *Appl. Mech. Rev.* **66(3)**, 030,802 (2014)
 30. Genin, L.G., Zhilin, V.G.: Influence of a longitudinal magnetic field on the friction in a pipe flow of mercury (in Russian). *Teplofiz. Vys. Temp.* **4**, 233 (1966)
 31. Molokov, S., Bühler, L.: Liquid metal flow in a U-bend in a strong uniform magnetic field. *J. Fluid. Mech.* **267**, 325–352 (1994)
 32. Reimann, J., Barleon, L., Buceniaks, I., Bühler, L., Lenhart, L., Malang, S., Molokov, S., Platnieks, I., Stieglitz, R.: Magnetohydrodynamic investigations of a self-cooled Pb-17Li nblanket with poloidal-radial-toroidal ducts. *Fusion Eng. Des.* **27**, 593–606 (1995)